Supervised Classification For Analysis Of Cryospheric Zones Using SAR Statistical Timeseries

Christophe Lin-Kwong-Chon, Matthieu Gallet, Suvrat Kaushik, Emmanuel Trouvé

SUPERVISED CLASSIFICATION FOR ANALYSIS OF CRYOSPHERIC ZONES USING SAR STATISTICAL TIMESERIES

Christophe Lin-Kwong-Chon[†], *Matthieu Gallet*[†], *Suvrat Kaushik*[†], *Emmanuel Trouvé*[†]

[†] : Université Savoie Mont Blanc, LISTIC, Annecy, France
Contact : {firstname.lastname}@univ-smb.fr

ABSTRACT

This study explores machine learning for classifying X-band Synthetic Aperture Radar (SAR) monovariate time series from four cryospheric zones in the Mont-Blanc massif. We aim to classify ablation zones, accumulation zones, hanging glaciers, and ice aprons using log-cumulants and Dynamic Time Warping Barycentric Averaging. Our approach evaluates distances between time series and estimated reference centroids, employing HH and HV polarimetric channels. We propose an extension to this method by aggregating class membership probabilities from selected polarimetric combinations. Results are compared across polarimetric channels, revealing insights into classification performance.

***Index Terms*—** SAR, Glaciers, Cryospheric zones classification

1. INTRODUCTION

SAR satellites, such as PAZ, are instrumental in monitoring cryospheric zones and crucial for understanding climate change due to their ability to observe icy areas under various weather conditions [1]. The classification of glaciers, a complex task due to their spatiotemporal variability, leverages distinctive patterns and physical multimodalities, with recent methodologies employing a variety of textural features and surface measurements for effective results [2, 3].

Deep learning methods have achieved high-performance results, particularly when using data from multiple sources and large, complex learning models. However, these methods require a large amount of data and struggle with the small surface areas of high mountain glaciers and limited labeled samples [4]. Despite these challenges, high-resolution imaging allows the identification of even small glaciers, with the X-band's sensitivity to surface and sub-surface variations enabling the detection of surface changes and water content [5, 6, 7, 8]. A recent study suggests the promising potential of combining HH/HV channels with backscattering coefficient σ_0 and Pauli decomposition for glacier classification [9].

Univariate statistics such as log-cumulants have proven effective in SAR data classification by synthesizing spatial information and exhibiting robustness against speckle-type multiplicative noise [10, 11]. To address temporal distortions resulting from the topographic and geographic specificities of the studied zones, approaches like Dynamic Time Warping (DTW) have been proposed to establish similarity between time series. Extending this method to compute the centroid of time series using the DTW Barycenter Averaging (DBA) method allows temporal information to be synthesized while reducing computational costs during inference [12, 13].

In this study, we aim to explore a machine-learning approach based on the classification of monovariate time series from X-band SAR images relating to four types of cryospheric zones within the Mont-Blanc massif. Our objective is to classify the following classes: ablation zones, accumulation zones, hanging glaciers, and ice aprons. The evaluation is conducted through a majority vote on DTW distances between the time series of the first three log-cumulants and their centroids estimated by DBA during training, for each of the considered classes, specifically for the HH and HV polarimetric channels. To leverage both polarimetric channels, we propose extending the majority vote by aggregating the probability of class membership based on statistics for a one optimal polarimetric combination. Finally, the obtained results are compared with the two polarimetric channels separately.

2. SAR DATASET FOR MACHINE LEARNING

Study site: The study area considered is the Mont-Blanc massif, located in the Northern Alps, France, as illustrated in Figure 1. Twenty-nine images from the PAZ satellite in X-band with dual polarizations (HH and HV) were acquired between January 1, 2020, and December 31, 2020, at a spatial resolution under 3 meters and a temporal resolution of approximately 11 days. The data were subjected to a simple radiometric calibration to retain only amplitude information. The four cryospheric classes considered, illustrated in Figure 2, are as follows: Ice Aprons (ICA) are small (typically $<$ 0.009 km^2 in the Mont-Blanc massif) and irregularly shaped thin ice patches found above the regional Equilibrium Line Altitude (ELA) on steep slopes (typically between $40°$ and $65°$). In addition, valley glaciers encompass accumulation areas (ACC), where the snow turns into firn and ice, and ablation areas (ABL) characterized by bare ice after snowmelt.

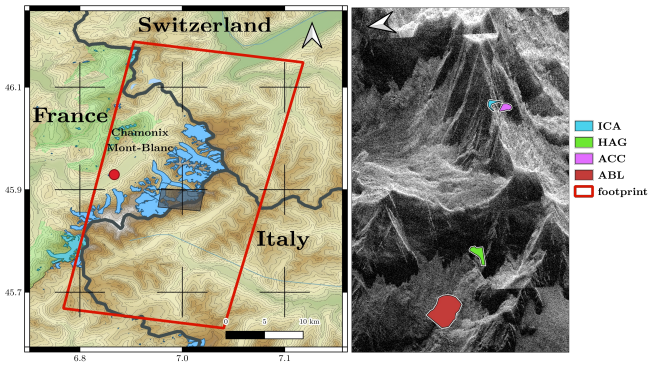

Fig. 1: Mont-Blanc massif with the footprint of PAZ acquisitions. The grey rectangle in the left map corresponds to the PAZ image displayed on the right.

Finally, Hanging glaciers (HAG) are smaller detached glaciers located in cirques or on steep slopes.

Dataset: A set of Regions of Interest (ROIs) were manually selected from optical images and projected into radar geometry to minimize geometric distortions due to the projection of a complete SAR image from a medium-resolution DEM (IGN 10m). The ROIs are then sliced into fixed-size windows of 11 by 11 pixels (approximately corresponding to a size of 33 m square), without overlap, for the complete temporal series. This patch size is a trade-off between the maximum number of samples per class and a sufficiently large contextual area. Data balancing is achieved by undersampling the minority class. This approach aims to correct imbalances in class distribution, ensuring no bias towards over-represented classes and the ability to generalize efficiently to all classes. Finally, each class contains 33 samples distributed among 3 to 7 geographically distinct groups forming a dataset of size 11 by 11 pixels by 29 acquisitions, and 2 polarimetric channels (HH and HV). The dataset can be found online[1].

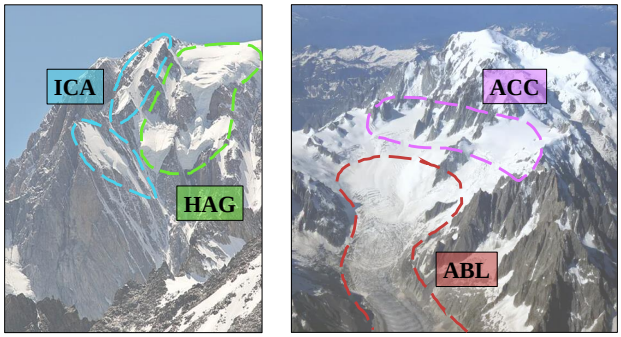

Fig. 2: Illustration of accumulation, ablation (*Tofig, Rashidov*. East face of the Mont Blanc), and hanging glacier, ice apron (*Simo, Räsänen*. South East face of Mont Blanc).

[1]https://zenodo.org/records/10401360

3. METHODOLOGY

3.1. Features selection

We explore a set of combinations of the two polarimetric channels, HH and HV, drawing inspiration from polarimetric decompositions and indices calculated in the context of multispectral data. This exploration is carried out through cross-validation, aiming to identify an index sensitive to cryospheric type changes. For the sake of brevity, we only present the most effective combinations. The first three log-cumulants [10], denoted as κ_1, κ_2, and κ_3, are used to reduce data dimensionality and synthesize spatial information on each raw or combined polarimetric channel. These statistics are calculated for each window of size 11 by 11 pixels, for each acquisition. Thus, for a window of size $n \times n$ and a time series of length m, we obtain a vector of size $3 \times n \times n \times m$.

3.2. Architecture

The proposed method is built on two parts as illustrated in Figure 3. The first part is a centroids estimation with the DBA and the second part is a probability classification using the statistical distance matrix. DTW is an effective measure of the similarity between two sequences, regardless of the dynamics involved, making it robust to shift or different acquisition times that may differ between samples, as is particularly the case with SAR data. We propose constraining the DTW, and by extension the DBA, by implementing the Sakoe-Chiba constraint with a radius of 3. This constraint window enables the search for the optimal matching sample within a timeframe of 3 samples or approximately 1 month.

DBA centroid estimation: As presented in Figure 3, the first step consists to estimate the centroids or barycenters $B_{c,k}(t)$ for each class c and for each statistic k using the DBA method [13]. DBA is designed for aligning time sequences taking into account time series derivatives. The objective is to reduce the total squared DTW distances between the average sequence and the collection of sequences.

Probability prediction: For a new sample, the distance matrix of time series barycenters M is defined as follows:

$$M = \begin{bmatrix} \mathcal{D}\left(B_{0,0}, s_0(t)\right) & \cdots & \mathcal{D}(B_{0,k}, s_k(t)) \\ \vdots & \ddots & \vdots \\ \mathcal{D}(B_{c,0}, s_0(t)) & \cdots & \mathcal{D}(B_{c,k}, s_k(t)) \end{bmatrix} \quad (1)$$

where $\mathcal{D}$ denotes the similarity measurement DTW, the vector $s_k(t)$ the temporal training sample for the k-th statistics.

Since statistics have different dynamics, each statistical distance vector is individually analyzed. The probability of belonging to a class is determined by counting the number of times that class yields the minimum distance among the considered classes for each statistic. This count is then normalized by the number of statistics considered. The predicted class is the one with the highest probability. As a result, four

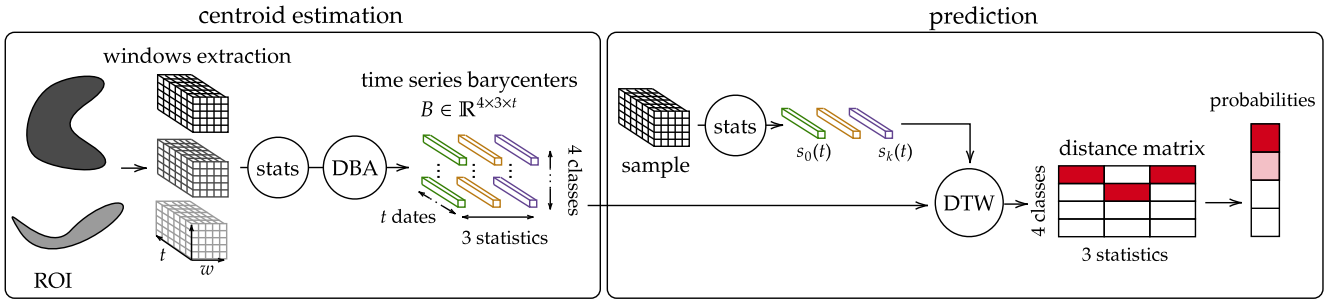

Fig. 3: Statistical DBA classification

types of probabilities can be identified for a distance matrix of 3 statistics: 100%, 66%, 33%, and 0%.

3.3. Experiments

The amount of data is very small, nevertheless, to ensure the robustness of the method, a leave-one-group-out cross-validation is conducted. The idea is to use all samples from all groups for the estimation of barycenters, except those from a single group. These are reserved for evaluation. As the groups are geographically distinct, this ensures that the training and test samples are not spatially correlated. This procedure is carried out for each group in the dataset. The average performances are calculated by stacking the results of each group against the ground truth. Four scenarios are presented here, the two baselines **S1**, **S2** respectively the individual polarimetric channels HH and HV, one additive combination $\mathbf{S3} = HH + HV$, and the best found combination, the normalized cross-polarisation ratio given by: $\mathbf{S4} = (HH - HV)/(HH \cdot HV)$.

4. RESULTS

The objective is to investigate channel combinations that yield the most effective classification. Firstly, the results are presented in terms of classification performance, F1-score and overall accuracy, then a cross-validation inferences regarding prediction zones.

4.1. Cryopheric classification

Table 1 shows a comparison of F1 scores for the four scenarios. The bold values identify for each class which scenarios yielded the best performance. The initial scenarios, identified as single-band polarimetric **S1** and **S2**, show good performance in the ablation and ice apron classes, but have limitations in accurately classifying the hanging glacier class. The introduction of the additive ratio in **S3** improves the classification problems observed in mono-polarimetric bands. On the other hand, **S4**, which presents the best polarimetric ratio, delivers significantly better and more consistent results for all four classes.

In particular, there is a 45% improvement in the HAG class compared to the mono-polarimetric bands. Despite the relatively limited data set and resolution imagery, the normalized cross-polarization ratio in **S4** provides an insightful initial classification for these small glaciers. Although the combination of the three best polarimetric ratios does not exceed the F1 scores of **S4**, it still outperforms the basic solutions, emphasizing its effectiveness in improving classification results.

4.2. Glaciers inference

During cross-validation, the prediction group is used to evaluate the classification, but also to obtain inference. The results for each class are shown in Figure 4 and are obtained via **S4**. The figure illustrates distinct classes, including the ablation zone, accumulation zone, hanging glacier zone, and ice apron zone, arranged from top to bottom. All rasters are in radar geometry, and the PAZ SAR image of June 21, 2020, is displayed on the left as an illustration of input data.

Upon analyzing all pixels obtained through inference, there is an uneven distribution, with a predominance of predictions for ABL and HAG. The ablation zone exhibits a highly uniform mapping prediction. This is because of the specific physical characteristics of glacier ablation zones (presence of crevasses, debris, and bare ice). These physical attributes are not commonly observed with the other classes. Confusion between the remaining three glacier classes (ACC, HAG, and ICA) is understandable, as these classes show similar physical and topographic attributes. These classes occur generally above the regional Equilibrium Line Altitude (ELA), on steeper slopes, and are generally covered with a layer of snow. The accumulation zones of glaciers were found

Table 1: Comparison of F1-score and accuracy performances (in %) between different classes and test scenarios.

	ABL	ACC	HAG	ICA	Accuracy
S1	37.50	9.09	0.00	30.51	20.45
S2	**45.16**	3.64	0.00	26.23	22.73
S3	39.47	**24.14**	8.51	26.51	26.52
S4	38.96	20.41	**45.33**	**31.75**	**35.61**

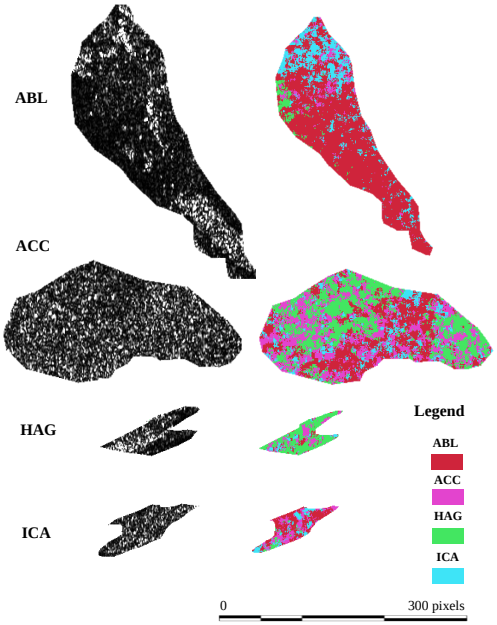

Fig. 4: Inference results with the S4 model on testing groups (ABL005, ACC005, HAG004 and ICA002).

to be the most difficult to distinguish because it does not provide any unique distinguishing physical characteristics that can aid its classification. However, the hanging glacier zone demonstrates a highly homogeneous mapping prediction. Results for hanging glaciers provide us with a very encouraging outcome, as this glacier class can easily be confused with the accumulation zones because of their similar physical nature. Finally, the ice apron zone, similar to the ABL zone, shows moderate confusion. Since ICAs are very closely associated with the ACC zone of glaciers, and their behavior can also be similar to glacier ABL zones in the summer [8], this is a very difficult class to distinctively classify.

These results demonstrate the classification and inference capabilities of the DTW DBA method, with a optimal polarimetric combination. Despite the small size of classified areas and limited data availability, the performance in large zone like ABL and small zones like HAG is improved by the joint use of log cumulants and polarimetric combination. However, an observed imbalance in the classification of ACC and ICA highlights the need for improvement in future research.

5. CONCLUSIONS

Spatio-temporal classification of a small data set, with a focus on small glaciers, is a challenging task. In this paper, classification is performed from SAR X-band high resolution image time series through the search for reference centroids for each class, and dynamic temporal wrapping distance. Our study focused on combining and enhancing the value of polarimetric ratios using a counting metric. The classification results showed promising performance, reaching accuracy levels of the order of 30-40%. Moreover, our inference results demonstrated the generalization capabilities of the method, a crucial aspect given the small size of our dataset. However, it is important to note the difficulties encountered during classification, including noticeable confusion patterns. Ongoing efforts will focus on refining these results, and addressing the complexities inherent in classifying small glaciers.

Acknowledgement The authors would like to thank the *Spanish Instituto Nacional de Tecnica Aerospacial* (INTA) for the PAZ images (Project AO-001-051). The work was conducted as part of the SHARE CNES/PNTS project.

6. REFERENCES

[1] S. H. Winsvold, A. Kääb, C. Nuth, L. M. Andreassen, W. J.J. Van Pelt, and T. Schellenberger, "Using SAR satellite data time series for regional glacier mapping," *The Cryosphere*, vol. 12, no. 3, pp. 867–890, 2018.

[2] J. Arigony-Neto, F. Rau, H. Saurer, R. Jaña, J.C. Simões, and S. Vogt, "A time series of SAR data for monitoring changes in boundaries of glacier zones on the antarctic peninsula," *Annals of Glaciology*, vol. 46, pp. 55–60, 2007.

[3] Y. Lu, Z. Zhang, and D. Huang, "Glacier mapping based on random forest algorithm: A case study over the Eastern Pamir," *Water (Basel)*, vol. 12, no. 11, pp. 3231, Nov. 2020.

[4] R. Panwar and G. Singh, "Classification of glacier with supervised approaches using PolSAR data," *Environ. Monit. Assess.*, vol. 195, no. 1, pp. 58, Nov. 2022.

[5] J R Leigh, C R Stokes, R J Carr, I S Evans, L M Andreassen, and D J A Evans, "Identifying and mapping very small (¡0.5 km^2) mountain glaciers on coarse to high-resolution imagery," *J. Glaciol.*, vol. 65, no. 254, pp. 873–888, Dec. 2019.

[6] S. Kaushik, S. Leinss, L. Ravanel, E. Trouvé, Y. Yan, and F. Magnin, "Monitoring hanging glacier dynamics from SAR images using corner reflectors and field measurements in the Mont-Blanc massif," *ISPRS Ann. Photogramm. Remote Sens. Spat. Inf. Sci.*, vol. V-3-2022, pp. 325–332, May 2022.

[7] S. Kaushik, L. Ravanel, F. Magnin, E. Trouvé, and Y. Yan, "Ice aprons in the Mont-Blanc massif (western european Alps): Topographic characteristics and relations with glaciers and other types of perennial surface ice features," *Remote Sensing*, vol. 14, no. 21, pp. 5557, 2022.

[8] S. Kaushik, B. Cerino, E. Trouvé, F. Karbou, Y. Yan, L. Ravanel, and F. Magnin, "Analysis of the temporal evolution of ice aprons in the Mont-Blanc Massif using X and C-band SAR images," *Frontiers in Remote Sensing*, vol. 3, 2022.

[9] B. Barzycka, M. Grabiec, J. Jania, M. Blaszczyk, F. Pálsson, M. Laska, D. Ignatiuk, and G. Adalgeirsdottir, "Comparison of three methods for distinguishing glacier zones using satellite SAR data," *Remote Sensing*, vol. 15, no. 3, 2023.

[10] JM. Nicolas and S. N. Anfinsen, "Introduction to second kind statistics: Application of log-moments and log-cumulants to the analysis of radar image distributions," *Trait. Signal*, vol. 19, no. 3, pp. 139–167, 2002.

[11] F. E. A. Nogueira, R. C. P. Marques, and F. N. S. Medeiros, "SAR image segmentation based on unsupervised classification of log-cumulants estimates," *IEEE Geoscience and Remote Sensing Letters*, vol. 17, no. 7, pp. 1287–1289, 2020.

[12] H. Sakoe and S. Chiba, "Dynamic programming algorithm optimization for spoken word recognition," *IEEE transactions on acoustics, speech, and signal processing*, vol. 26, no. 1, pp. 43–49, 1978.

[13] F. Petitjean, A. Ketterlin, and P. Gançarski, "A global averaging method for dynamic time warping, with applications to clustering," *Pattern Recognition*, vol. 44, no. 3, pp. 678–693, 2011.